1992

Hamiltonian Chaos III

Niraj Srivastava

Charles Kaufman
University of Rhode Island, ckaufman@uri.edu

Gerhard Müller
University of Rhode Island, gmuller@uri.edu

Citation/Publisher Attribution

N. Srivastava, C. Kaufman and G. Müller. *Hamiltonian chaos III*. Computers in Physics **6** (1992), 84-88. Available at: http://dx.doi.org/10.1063/1.4823048

Hamiltonian Chaos III

Hamiltonian Chaos III

Niraj Srivastava, Charles Kaufman, Gerhard Müller

Department of Physics, University of Rhode Island, Kingston, RI 02881-0817.

Does quantum chaos exist? If it exists, what is it? If it does not, what was it supposed to have been? Why should we associate chaos with a "third revolution in physics" if it fails to be expressible in terms of quantum mechanics, our most fundamental theory of physical reality? Is there something wrong with quantum mechanics? Or is chaos merely a mathematical construct relevant only for models in classical mechanics? Is the human mind doomed to interpret and understand quantum mechanics in classical terms? The list of unanswered questions in quantum chaos research itself shows symptoms of the phenomenon it attempts to grasp.[1]

How do we recognize *classical* Hamiltonian chaos? We have dealt with this question in our two previous columns.[2,3] In Part I we discussed the implications of integrability and non-integrability for the phase-space trajectories of classical Hamiltonian systems with two degrees of freedom. We described the method of *Poincaré surfaces of section* as a convenient and striking discriminant between the two possibilities. In Part II we searched for an alternate mode of representation for classical Hamiltonian systems, a mode that is an equally powerful indicator of chaos, but one that can be more directly translated into quantum mechanics than the Poincaré map. We proposed a representation based on the construction of *classical invariants* via time averages of dynamical variables, a representation that can be employed under very general circumstances including integrable and nonintegrable models. In this column we shall construct *quantum invariants*, demonstrate the impact of non-integrability on these quantities, and discuss their properties in relation to their classical counterparts. In a future column we intend to introduce *quantum Poincaré surfaces of section* for stationary states and bring full circle our survey of quantum and classical Hamiltonian chaos.

Consider a quantized integrable model. Its eigenstates are labeled by quantum numbers. There are as many quantum numbers as there are degrees of freedom. Each quantum number represents a quantized action. In the still evolving language of quantum chaos, quantum numbers are said to have been "lost" in the transition from a quantum system whose classical counterpart is integrable to one whose counterpart is chaotic. The broken, or lost, tori of classical chaos become lost quantum numbers of quantum chaos. As we shall see, the loss of quantum numbers is vividly mirrored in the behavior of the quantum invariants.

We begin by describing the construction of the quantum invariants for a

Hamiltonian $\hat{H}$. First find the energy eigenvalues E_n and eigenfunctions $|n>$ of $\hat{H}$. Then consider a dynamical variable, $\hat{D}(t)$, that is independent of $\hat{H}$. The matrix elements of $\hat{D}(t)$ in the energy representation are

$$<n|\hat{D}(t)|n'> = <n|\hat{D}|n'> \exp[i(E_n - E_{n'})t/\hbar].$$

We can take their time average to produce a time-independent (invariant) quantity. The off-diagonal elements $<n|\hat{D}(t)|n'>$ $(n \neq n')$ all have zero average value, so the time-averaged matrix is diagonal. (If there is degeneracy, the eigenvectors in the invariant subspaces must be chosen such that the off-diagonal elements are zero.) Just as each trajectory of a classical model leads to one value of the invariant associated with a given dynamical variable, each eigenstate of the Hamiltonian leads to a value of the *quantum* invariant,

$$D_n = \lim_{T\to\infty} \frac{1}{T} \int_0^T dt <n|\hat{D}(t)|n>. \tag{1}$$

associated with the dynamical variable $\hat{D}$.

As an illustration, think of the simple pendulum of mass m and length L (see Part II). The classical Hamiltonian is $p^2/2M + \Gamma(1-\cos\theta)$, where $p = M\dot{\theta}$, $\Gamma = mgl$, and $M = mL^2$. In Part II we chose the kinetic energy $K = \frac{1}{2}M\dot{\theta}^2$ as a dynamical variable. The invariant $I_K(E)$ associated with it, the average of K over one cycle, was found as a function of energy. We also found the allowed energies E_n implied by the Bohr-Sommerfeld procedure. This semi-classical quantization is not limited to the energy. For example, the quantized values of the kinetic energy are given by $I_K(E_n)$, which might therefore be called a semi-classical invariant.

For the determination of the true quantum invariant, it is necessary to find the eigenfunctions and eigenvalues of the quantized version of the pendulum Hamiltonian, which is

$$\hat{H} = -\frac{\hbar^2}{2M}\frac{d^2}{d\theta^2} + \Gamma(1-\cos\theta), \tag{2}$$

and then to evaluate the expectation value $K_n = <n|-(\hbar^2/2M)d^2/d\theta^2|n>$ of the kinetic energy operator. (The question of agreement between these two methods, i.e., the validity of the semi-classical procedure for the simple pendulum, is very illuminating and will be considered separately.) The effect of either kind of quantization is the replacement of the continuous curve $I_K(E)$ by the discrete set of points (K_n, E_n). Fig. 1 shows the piecewise smooth function $I_K(E)$ obtained from classical time averages, and the set of points (K_n, E_n) obtained from quantum time averages. Except for the immediate vicinity of the classical separatrix, the set of points follows the continuous curve almost exactly. Remember that each point on the line $I_K(E)$ represents a classical invariant torus in phase space, while each dot on the chain (K_n, E_n) represents a quantized torus. Quantization is seen to force all the "orbits" in a phase space volume $\hbar$ to coalesce into a single quantum state.

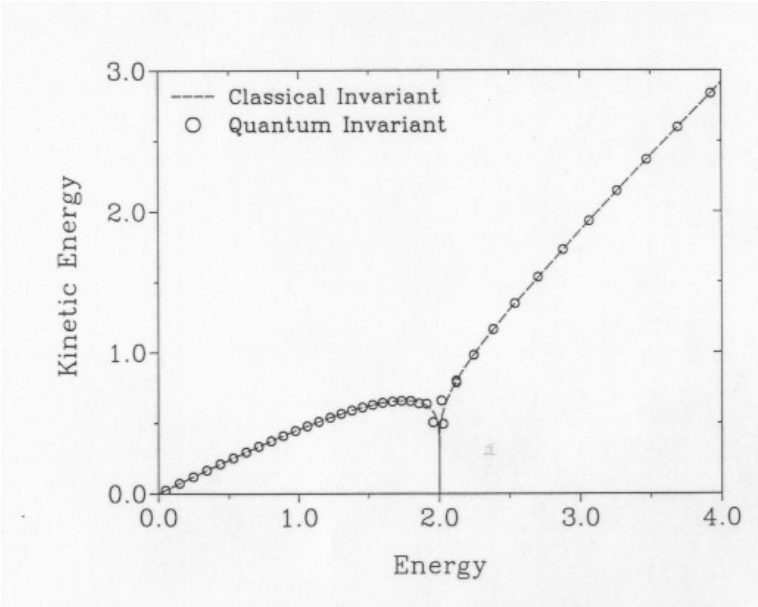

Figure 1: Classical invariant and quantum invariant for the simple pendulum. The solid line $I_K(E)$ is the average kinetic energy over one period, as a function of the total energy E for $0 \leq E \leq$ 10 mgL(see Part II). The circles are the points (K_n, E_n), where E_n is the energy eigenvalue and K_n is the diagonal element of the kinetic energy operator in the energy representation.

We need to consider two degrees of freedom to study chaos. The uncertainty principle replaces the continuum of classical states within a volume $\hbar^2$ by a single quantum state; the dots defined by pairs of independent invariants tend to form a two-dimensional (2d) web. We now explore the implications of the correspondence principle for the structure of this *invariant-web*.

Recall the thermodynamic analogy of Part II. A 2d system has at most two independent invariants and any further invariant is expressible in terms of the two independent ones. We pictured this relationship as an equation of state or alternatively as a surface $z(x, y)$, where x and y are independent variables. If a classical 2d system has only one analytic invariant, or if it is not known whether a second one exists, we use numerical invariants instead. These numerical time averages produce a piecewise smooth function when there is a second independent analytic invariant. This *invariant-surface* is the classical version of the invariant-web.

A simple 2d example whose classical version is integrable is the particle in a box:

$$V = \begin{cases} 0, & 0 < x < a,\ 0 < y < b \\ \infty\ , & \text{otherwise.} \end{cases} \tag{3}$$

The eigenstates $|n_1 n_2>$ are labeled by the integers n_1 and n_2 and the allowed

energies are

$$E_{n_1,n_2} = (n_1^2/a^2 + n_2^2/b^2)(h^2/8m),$$

with $n_1,\ n_2 = 1, 2, 3, 4, \ldots$. We can construct two invariants from the dynamical variables $\hat{I}_1 = (\hbar^2/2m)\,\partial^2/\partial x^2$ and $\hat{I}_2 = (\hbar^2/2m)\,\partial^2/\partial y^2$. Each state may then be labeled by its values of $I_1 = <n_1 n_2|\hat{I}_1|n_1 n_2>$ and $I_2 = <n_1 n_2|\hat{I}_2|n_1 n_2>$ instead of by n_1 and n_2. In this example, the diagonal elements can be found exactly and I_1 and I_2 are $-\pi^2\hbar^2 n_1^2/(2ma^2)$ and $-\pi^2\hbar^2 n_2^2/(2mb^2)$ respectively. The web formed by the set of points (I_1, I_2) is a net whose mesh size increases in each direction. Finally, suppose we chose as dynamical variables the operators $\hat{D}_1$ and $\hat{D}_2$ corresponding to the actions D_1 and D_2 of the classical problem. The invariants are $I_{D_1} = n_1\hbar$ and $I_{D_2} = n_2\hbar$. Each mesh in the (I_{D_1}, I_{D_2}) web is a square of side $\hbar$. For each set of invariants used, the classically allowed continuum of states would be seen to coalesce into discrete states, exactly as it does in the 1d case. In this integrable example, the states form a perfectly regular web.

In a more complicated example, when the invariants are unknown or perhaps nonexistent, this procedure fails. We rescue it with numerical invariants. Each eigenstate can be labeled by a pair of numerical invariants, say (E_n, D_n), constructed as in the above. We can now draw the scatter diagram of these pairs in the (E, D) plane, in spite of the fact that a second *analytic* invariant in the classical problem might not exist. A regular mesh will signal an integrable problem; disorder signals chaos.

We apply this procedure to a quantized system of two interacting identical spins whose Hamiltonian can be expressed as[4–6]

$$\hat{H} = \hbar^2 \sum_{\alpha=x,y,z} \left(-J_\alpha \hat{\sigma}_{1\alpha}\hat{\sigma}_{2\alpha} + \frac{1}{2} A_\alpha \left(\hat{\sigma}_{1\alpha}^2 + \hat{\sigma}_{2\alpha}^2 \right) \right). \tag{4}$$

The operators $\hat{\sigma}$ satisfy the angular momentum commutation rules

$$[\hat{\sigma}_{i\alpha}, \hat{\sigma}_{j\beta}] = i\delta_{ij} \sum_\gamma \epsilon_{\alpha\beta\gamma}\, \hat{\sigma}_{i\gamma}. \tag{5}$$

The angular momentum operators corresponding to spins 1 and 2 are $\hat{\mathbf{S}}_1 = \hbar\hat{\sigma}_1$ and $\hat{\mathbf{S}}_2 = \hbar\hat{\sigma}_2$ respectively; $\hat{S}_1^2$ and $\hat{S}_2^2$ have eigenvalues $\sigma(\sigma+1)\hbar^2$, where $\sigma = 1/2, 1, 3/2, \ldots$. If we take the limits $\hbar \to 0$ and $\sigma \to \infty$, such that the product $\sigma(\sigma+1)\hbar^2$ remains constant, and replace the operators $\hat{\mathbf{S}}_i$ by the vectors $\mathbf{S}_i$, then $\hat{H}$ reduces to the classical Hamiltonian we have considered in Parts I and II, that is, a system of two classical three-component spins of fixed length. The classical integrability condition depends on the parameters J_α and A_α and is given in Part II. (We retain the notation J_x, J_y, J_z for the parameters at some slight risk of confusion with the actions J_1, J_2.)

Consider the integrable model $J_x = 1.2$, $J_y = 0.8$, $J_z = A_x = A_y = A_z = 0$. Choose $\sigma = 35$ and $\hbar$ such that $\sigma(\sigma+1)\hbar^2 = 1$. The smallest matrix representation for a single such spin is 71×71 and the matrix representation of the Hamiltonian is then $71^2 \times 71^2$. We diagonalize this matrix and find its

eigenvectors $|n>$ using the method described in Problem 1. Then we construct numerical invariants from $\hat{M}_\alpha^2 = \hbar^2(\hat{\sigma}_{1\alpha} + \hat{\sigma}_{2\alpha})^2/4$ with $\alpha = x, y, z$ and evaluate $\tilde{M}_{xn} = \sqrt{<n|\hat{M}_x^2|n>}$ and $\tilde{M}_{zn} = \sqrt{<n|\hat{M}_z^2|n>}$, where $|n>$ ranges through the 5041 eigenvectors of $\hat{H}$. The nth eigenstate is thus characterized by its energy E_n and by the invariants $\tilde{M}_{xn}$ and $\tilde{M}_{zn}$.

If we were to draw our surfaces using all these states, their structure would be rather opaque. The eigenstates of $\hat{H}$ fall into eight different symmetry classes, each having specific transformation properties under the action of the symmetry group of $\hat{H}$.[6] The patterns of the invariants are different from class to class. We segregate the eigenstates accordingly. Fig. 2a shows the points $(E_n, \tilde{M}_{zn})$ for each eigenstate of two of these classes only. The pattern is very intriguing. The array of points is highly structured and is apparently a fully intact 2d invariant-web with four bonds per vertex. In the plane of the (unknown) action coordinates J_1 and J_2, all the tori in a square of area $\hbar^2$ would be quantized into a single state analogous to our earlier example. There exists a (nonlinear) mapping between these squares in the (J_1, J_2) plane and the meshes of the invariant-web in the (E, M_z) plane, guaranteed by the classical integrability property. It is given by the pair of functions $E(J_1, J_2)$ and $M_z(J_1, J_2)$. Even if we do not know these functions, their existence means the web exists in both the (E, M_z) and the (J_1, J_2) planes. Every thread of a web can then be interpreted as a line of constant action. Moving along one such line, each successive intersection marks a change of $\hbar$ in the other action.

Recall that the classical frequency of the angle variable ω_i is given by $\omega_i = \partial E(J_1, J_2)/\partial J_i$. Now observe the set of nearly vertical threads of Fig. 2a. Moving from bottom to top, the slope of a thread changes from positive to negative, passing through a point of infinite value. If we interpret this thread as a line of constant J_2, its slope is $1/\omega_1$, so we see ω_1 slows down to zero at the point of infinite slope. Zero frequency in the classical action plane marks a separatrix. When an integrable classical problem has a small nonintegrable perturbation added to it, chaos is most obvious near the separatrices. So it is in this region of the plane of quantized actions where we expect chaos to be most conspicuous. If we think of the function $E(J_1, J_2)$ as defining a surface above the (J_1, J_2) plane, we have our topographic map of quantized actions, and we anticipate that evidence for chaos should be sought along its ridges and valleys.

For comparison we present the classical counterpart of this map, produced as in Part II, using the corresponding classical Hamiltonian and dynamical variables. Pick an initial condition. Evaluate the time averages of $M_x^2 = (S_{1x} + S_{2x})^2/4$ and $M_z^2 = (S_{1z} + S_{2z})^2/4$ along the trajectory that evolves from that initial condition. Repeat the process for another initial condition, and another, etc. For convenience we adopt the notation $\tilde{M}_x = \sqrt{<M_x^2>}$ and $\tilde{M}_z = \sqrt{<M_z^2>}$. Fig. 2b is the plot of the pairs $(E, \tilde{M}_z)$ obtained by carrying out this averaging procedure for 5146 randomly chosen trajectories (cf. Fig. 4a of II). It is very similar to the quantum picture shown in Fig. 2a. Fig. 2b can be thought of as the projection onto the $(E, \tilde{M}_z)$ plane of the surface defined by the equation of state $\tilde{M}_x = \tilde{M}_x(E, \tilde{M}_z)$. We exhibit the surface more con-

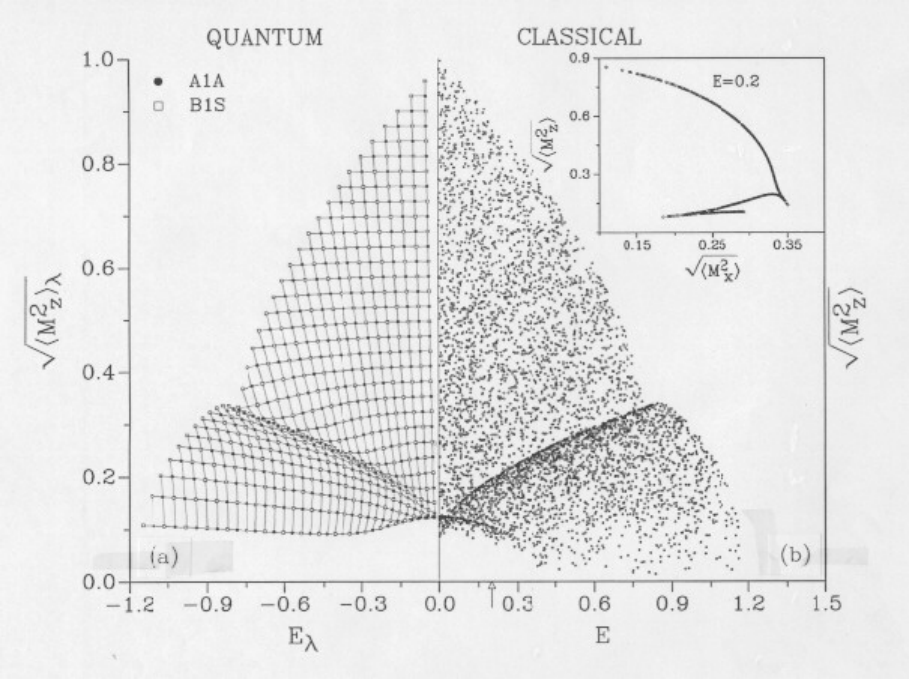

Figure 2: (a) Quantum invariant $\tilde{M}_{zn} = \sqrt{<n|\hat{M}_z^2|n>}$ versus eigenvalue E_n for two of the symmetry classes of states (full circles and open squares) of the integrable case $J_x = 1.2$, $J_y = 0.8$, $J_z = A_x = A_y = A_z = 0$ of the quantum spin model (4) for $\sigma = 35$. The total number of states shown is 595. (b) Classical invariant surface $E(\tilde{M}_x, \tilde{M}_z)$ projected onto the $(E, \tilde{M}_z)$ plane. The inset shows invariant $\tilde{M}_z$ versus invariant $\tilde{M}_x$ at energy $E = 0.2$. The points are time averages over individual trajectories for initial conditions randomly chosen in phase space (main plot) or on the energy hypersurface (inset). The number of data points is 5,146 (projection, main plot) and 1,200 (section, inset).

vincingly, again as in Part II, in the inset to Fig. 2b, which is the intersection of the surface $E(\tilde{M}_x, \tilde{M}_z)$ with the plane $E = 0.2$. All points lie on a piecewise smooth line as anticipated. The cusps represent singularities in the (not explicitly known) functional dependence of $\tilde{M}_x$ and $\tilde{M}_z$ on J_1 and J_2. The folds in the invariant-surface produce a clearly visible shading effect in the projection of Fig. 2b.

Fig. 3 shows the complete set of invariant-webs for another integrable case, $J_x = 1.7, J_y = 0.3, J_z = A_x = A_y = A_z = 0$. Each one of the four webs shown contains only states from two of the eight symmetry classes. The spin quantum number in this illustration is $\sigma = 90$, yielding a total of 32,761 eigenstates. (We use $\sigma(\sigma + 1)\hbar^2 = 1$ as before.) We see again the perfectly regular patterns of the fully intact web in each case.

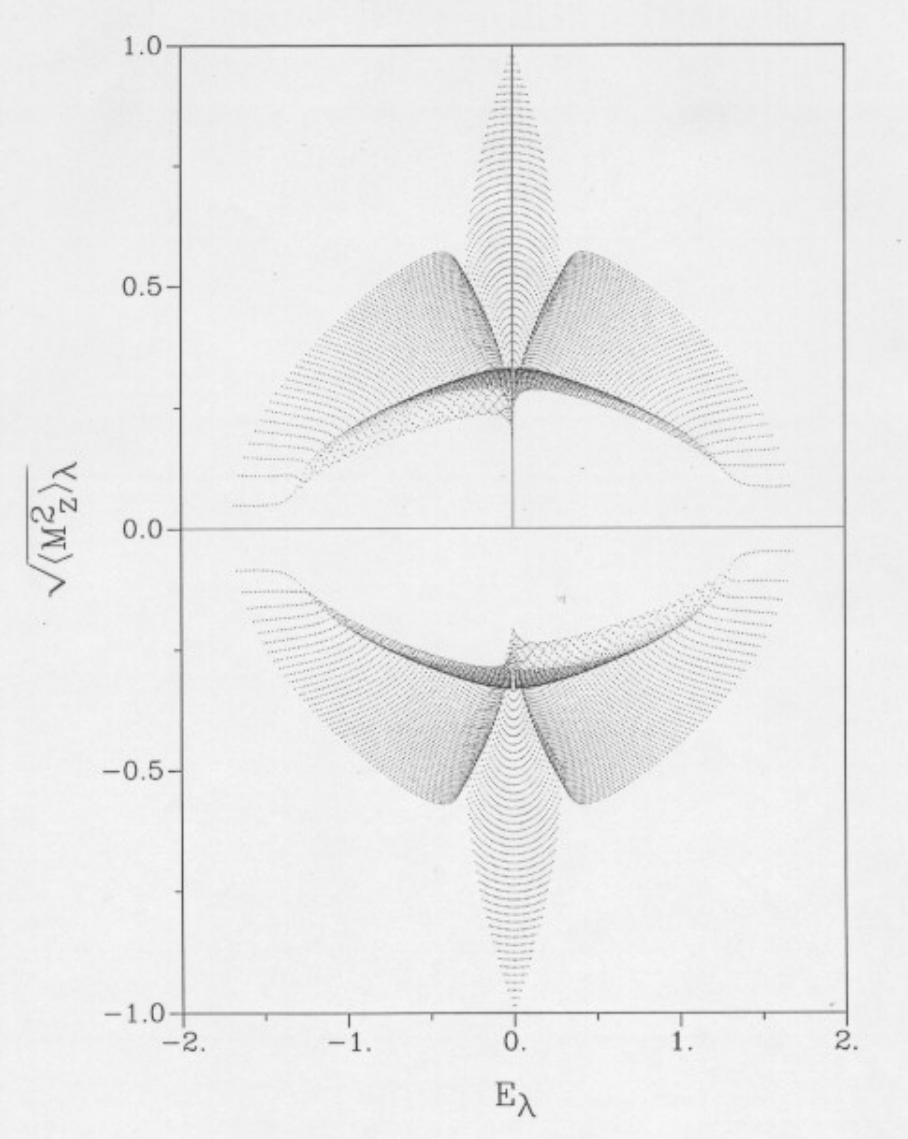

Figure 3: Quantum invariant $\tilde{M}_{zn}$ versus E_n for all symmetry classes of the integrable case $J_x = 1.7$, $J_y = 0.3$, $J_z = A_x = A_y = A_z = 0$ of the quantum spin model (4) for $\sigma = 90$. Only one quarter of the states for each class is shown. The total number of states shown is 16,256.

On to chaos. Fig. 4a is the topographic map of quantized actions for the nonintegrable system $J_x = J_y = 1$, $J_z = 0$, $A_x = -A_y = -0.7$, $A_z = 0$, again with $\sigma = 90$. Fig. 4b is the classical counterpart. Each map is symmetric about

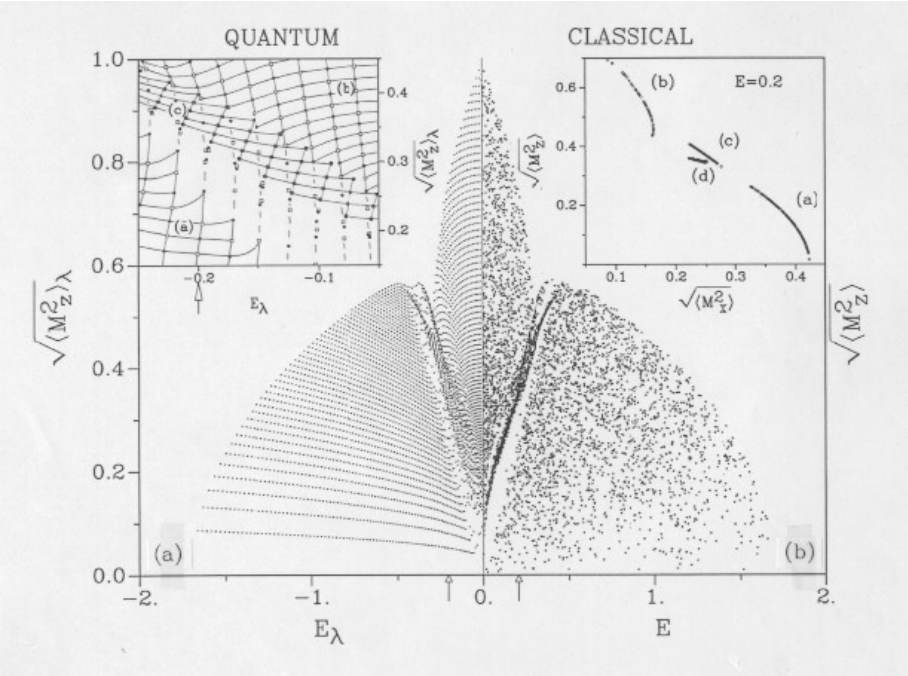

Figure 4: (a) Quantum invariant $\tilde{M}_{zn}$ versus E_n for the same symmetry classes A1A and B1S as in Fig. 2a, but for the non-integrable case $J_x = J_y = 1$, $A_x = -A_y = -0.7$, $J_z = A_z = 0$ for $\sigma = 90$. The total number of states shown is 4,005. The inset shows the same quantities for those states with $-0.25 < E < -0.05$, $0.1 < M < 0.5$, for the same Hamiltonian but for $\sigma = 45$. (b) Remnant of the classical invariant-surface $E(\tilde{M}_x, \tilde{M}_z)$ projected onto the $(E, \tilde{M}_z)$ plane, with the J's and A's as in (a). The inset shows $\tilde{M}_z$ versus $\tilde{M}_x$ at energy $E = 0.2$. The points are time averages over individual trajectories for initial conditions randomly chosen in phase space (main plot) or on the energy hypersurface (inset). The number of data points is 5,050 (projection, main plot) and 495 (section, inset).

the line $E = 0$, so only half of each map is actually shown; as before only states with the same symmetry are used. The correspondence is even more striking for this chaotic model than for the integrable one. The inset to Fig. 4a is an enlargement of a portion of the web. The quantum results show evidence of chaos just where we anticipated—where the threads become vertical and the classical separatrix is located. The signature is the destruction of the web. Of course the web is an artifice and we may join the dots as we wish. Just as the existence of two good quantum numbers assures the web's possibility, the loss of a quantum number assures the web's impossibility and a smooth, regular, natural joining of all the dots in the separatrix region cannot be accomplished. The quantum number that would tell us which way to go to the next dot on the

thread has been lost.

What about classical chaos? The invariant-surface has been destroyed in the same region. The projection shows blank spaces indicating breaks in the surface. The inset shows the intersection of the fragments of the invariant surface with the plane $E = 0.2$ and we see that the smooth curve of Fig. 2 has broken into pieces. Some of the pieces still *appear* smooth on the scale of the picture—regular "islands" in the chaotic sea. In the apparently regular regions of the bottom left and top right ((a) and (b) respectively), the invariant-web is fully intact. Here chaos (which must be present since there are broken tori everywhere when the system is non-integrable) is confined to areas much smaller than the mesh size. Between the two regular regions a broad band of chaos extends along a separatrix of the classical motion. Here the invariant-web is interrupted, and the quantum states cluster in short strips along the dashed lines (see inset). The quantum traces of the regular islands are separate webs, isolated from any others by the destroyed web of a separatrix. The web marked (c) in the inset is just one such island web. The island's classical counterpart can be easily recognized as the secondary KAM tori in the Poincaré section of Fig. 3b of Part II. Each of the other major fragments of the invariant-surface can be similarly identified.

By looking in the right place we have found clear quantum evidence for classical chaos. The price we have paid is computational. Fig. 2a required the diagonalization of a 32761×32761 matrix. Fig. 2b requires the separate numerical integration of the four canonical equations for 5146 different sets of initial conditions, each for as many as 100,000 integration steps. We believe the insight is worth the effort.

Suggested Problems for Further Study

1. The method for diagonalizing the spin Hamiltonian and calculating the invariants can be summarized as follows:
   (a) For ease of calculation express the Hamiltonian (see (4)) in terms of the raising and lowering operators $\hat{\sigma}_{\pm}$ rather than the Cartesian spin matrices $\hat{\sigma}_{x,y}$.
   (b) Use as a preliminary set of basis vectors the simultaneous eigenstates of $\hat{\sigma}_{1z}$ and $\hat{\sigma}_{2z}$.
   (c) Find the linear combinations of these basis vectors that are invariant under the symmetry operations which leave $\hat{H}$ invariant. See ref. 6 and therein for details.
   (d) Compute the matrix elements of $\hat{H}$ in the representation in which the linear combinations found in step (c) are the basis vectors. Because of the way the basis states were chosen, the new matrix will be in block-diagonal form. For a Hamiltonian of the form given in (4), there will be eight blocks.
   (e) Determine the eigenvalues E_n and eigenvectors $|n>$ for each block of the matrix found in step (d).
   (f) Find the diagonal elements $M^2_{xn} = <n|\hat{M}^2_x|n>$ and $M^2_{zn} = <n|\hat{M}^2_z|n>$

using the basis vectors $|n>$ found in step (e).
(g) Use each of the eight sets of values $(E_n, M^2_{xn}, M^2_{zn},)$ as the data from which to draw the webs.
Implement this method for a simpler Hamiltonian and for a smaller value of σ than used in the text. For example, start with the simple system of two spin $\frac{1}{2}$ objects whose Hamiltonian is $\hat{\sigma}_1 \cdot \hat{\sigma}_2$ and then go on to more involved systems and/or larger σ. The spin operators $\hat{\sigma}_1$ and $\hat{\sigma}_2$ each satisfy $\hat{\sigma}^2|n> = \frac{1}{2}(\frac{1}{2}+1)|n>$. We outline the procedure for $\hat{H} = \hat{\sigma}_1 \cdot \hat{\sigma}_2$.
(i) Enumerate all the states that are eigenstates of both $\hat{\sigma}_{1z}$ and $\hat{\sigma}_{2z}$, where $\hat{\sigma}_{1z}|+-> = \frac{1}{2}|+->$ and $\hat{\sigma}_{2z}|+-> = -\frac{1}{2}|+->$.
(ii) Enumerate the effect of the operators $\hat{\sigma}_{i\alpha}$ on each state. For example, $\hat{\sigma}_{1x}|+-> = \frac{1}{2}(\hat{\sigma}_{1+} + \hat{\sigma}_{1-})|+-> = \frac{1}{2}|-->$.
(iii) Find the 16 matrix elements of $\hat{H} = \hat{\sigma}_1 \cdot \hat{\sigma}_2$. For example, $<+-|\hat{H}|+-> = \frac{1}{2}$.
(iv) Find the eigenvalues E_n and orthonormal eigenvectors of $\hat{H}$. One of the eigenvalues is three-fold degenerate so you must find an orthogonal set of eigenstates in the corresponding 3d subspace.
(v) Use $\hat{M}^2_z \equiv (\hat{\sigma}_{1z} + \hat{\sigma}_{2z})^2$ as a second invariant. Find its diagonal matrix elements M^2_{zn} using the eigenvectors found in (iv).
(vi) Plot the scatter diagram of the (four) points M^2_{zn}, E_n. Note that since the symmetry group of $\hat{H} = \hat{\sigma}_1 \cdot \hat{\sigma}_2$ is not the same as that of the $\hat{H}$ of eq. (4), the block structure of the Hamiltonian matrix is different.

2. Solve the time-independent Schrödinger equation for the simple pendulum and use the wave function to find the values of the invariant arising from the potential energy. One method of solution is the "garden hose" method which consists of a numerical integration of the differential equation, from one end of the domain ($\theta = -\pi$) to the other ($\theta = \pi$), and the requirement that the wave function smoothly match at the two ends since the two ends are the same place. The energy, wave function, and slope at $\theta = -\pi$, are varied until this conditions is met. Another method consists of expanding the wave function in a convenient basis set to produce an explicit matrix for the Hamiltonian, and then numerically diagonalizing this matrix. Both methods are considerably facilitated by exploiting the definite parity of the solutions. Use the Bohr-Sommerfeld quantization condition to find the semi-classically allowed values of the potential energy. Compare these values to the above results in order to evaluate the validity of the semi-classical procedure.

3. This problem requires extensive precise numerical calculation to see the effects of the classical chaos on the quantum invariants. It differs from our spin examples because its phase space is not compact, and the number of states is not finite. Consider a particle in a stadium, i.e., a rectangle of lengths a and b, one of whose ends has been replaced by a segment of a circle, centered on the perpendicular bisector of the short sides, of radius R. Use an appropriate partial differential equation solver[7] to find

the eigenfunctions and eigenvalues for the corresponding time-independent Schrödinger equation. The wavefunctions can be used to find the values of the invariants I_1 and I_2 as discussed in the text. Here however, the matrix elements must be evaluated by numerical integration. Repeat for several values of R and plot the set of points (I_1, I_2) for each R. Initially choose $R >> a, b$. Then choose several smaller values of R so that the eigenvalues and eigenvectors would be significantly different than those for the rectangular stadium. Compare the resulting webs to those of the simple rectangle. This problem is a variation on the standard stadium problem[8,9] for which the box has semicircular ends and the integrable limit is the disk. In this example the integrable limit is the rectangle.

Acknowledgments. Quantum chaos research at URI is supported by the National Science Foundation, Grant DMR-90-07540. Access to supercomputers at the National Center for Supercomputing Applications, University of Illinois at Urbana-Champaign and at the NASA Ames Research Center is gratefully acknowledged. We thank Harvey Gould and Jan Tobochnik for helpful suggestions.

References

1. The atmosphere of excitement mixed with bewilderment in which current quantum chaos research takes place is best described in a research news story which appeared in *Science* **243**, 893 (1989) under the title "Quantum Chaos: Enigma Wrapped in a Mystery."

2. N. Srivastava, C. Kaufman, and G. Müller, *Comput. Phys.* **4**(5), 549 (1990). Referred to in the text as I.

3. N. Srivastava, C. Kaufman, and G. Müller, *Comput. Phys.* **5**(2), 239 (1991). Referred to in the text as II.

4. E. Magyari, H. Thomas, R. Weber, C. Kaufman, and G. Müller, *Z. Phys.* B**65**, 363 (1987).

5. N. Srivastava, C. Kaufman, G. Müller, R. Weber and H. Thomas, *Z. Phys.* B**70**, 251 (1988).

6. N. Srivastava and G. Müller, *Z. Phys.* B**81**, 137 (1990).

7. W. H. Press, B. P. Flannery, S. A. Teukolsky and W. T. Vetterling, *Numerical Recipes: The Art of Scientific Computing*, Cambridge University Press (1986); R. J. Riddell, Jr., *J. Comp. Phys.* **31**, 21 (1979)

8. G. Benettin and J.-M. Strelcyn, *Phys. Rev.* A**17**, 773 (1978).

9. S. W. McDonald and A. N. Kaufman, *Phys. Rev. Letts.* **42**, 1189 (1979); *ibid. Phys. Rev.* A**37**, 3067 (1988).